iScience

CellPress
OPEN ACCESS

Article

Convective thermal cloaks with homogeneous and isotropic parameters and drag-free characteristics for viscous potential flows

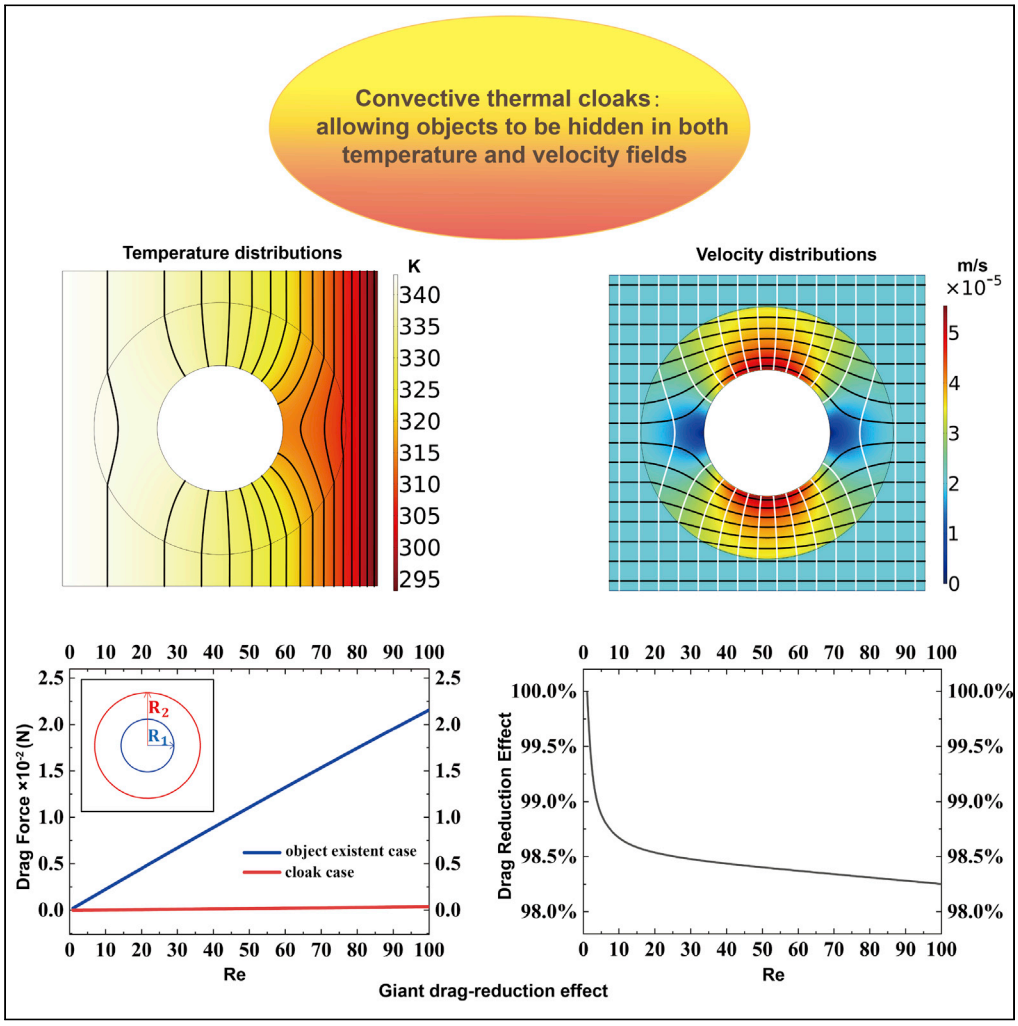

Nengzhi Yao, Hao Wang, Bin Wang, Xuesheng Wang, Jiping Huang

bwang@ecust.edu.cn (B.W.)
wangxs@ecust.edu.cn (X.W.)
jphuang@fudan.edu.cn (J.H.)

Highlights

Homogeneous and isotropic convective thermal cloaks are designed

The Reynolds number of flow fields increases about 100 times under zero drag

Convective thermal cloaks extend to non-creeping viscous potential flows

Yao et al., iScience 25, 105461
November 18, 2022
https://doi.org/10.1016/j.isci.2022.105461

iScience

CellPress
OPEN ACCESS

Article

Convective thermal cloaks with homogeneous and isotropic parameters and drag-free characteristics for viscous potential flows

Nengzhi Yao,[1] Hao Wang,[1] Bin Wang,[1,3,*] Xuesheng Wang,[1,*] and Jiping Huang[2,*]

SUMMARY

Although convective thermal cloaking has been advanced significantly, the majority of related researches have concentrated on creeping viscous potential flows. Here, we consider convective thermal cloaking works in non-creeping viscous potential flows, and propose a combination of the separation of variables method and the equivalent-medium integral method to analytically deduce the parameters of convective thermal cloaks with isotropic-homogeneous dynamic viscosity and thermal conductivity. Through numerical simulation, we demonstrate the cloaks can hide the object from thermo-hydrodynamic fields. Besides, by comparing the drag force cloaks bear in cloak case and the objects bear in object-existent case, we find convective thermal cloaks can considerably reduce the drag force, which appears drag-free characteristics. Finally, it is our hope that these developed methods can reduce the difficulties of metadevices fabrications, promote the development of drag reduction technology under higher Reynolds number, and shed light on the control of other multi-physics systems.

INTRODUCTION

Thermal cloaking has become key research issues in the development of modern military equipment and facilities,[1–4] such as aircrafts,[5,6] armor vehicles,[7,8] naval vessels,[9,10] and among others. As these researches involve the convective heat transfer closely, extending thermal cloaking from pure thermal conduction to convective heat transfer has played a critical role in thermal fluid motion community, which has facilitated the explorations in manipulating heat flux proactively as well.

Heat flux manipulation, a long-standing dream explored strenuously by numerous pioneers, has stepped into a new period since the transformation optics[11,12] developed into thermal field known as transformation thermodynamics.[13–15] Thereafter, various novel thermal metadevices have emerged, such as thermal cloaks,[16–19] thermal concentrators,[20–22] thermal rotators,[23–25] etc. Thermal cloaks, as their name implies, can thermally hide an object while maintaining the original distributions of the external thermal fields through regulating the thermal conductivity distributions. To validate the performances of thermal cloak practically, abundant experiments[24,26–31] have been conducted successfully via multiple artificial structures and materials known as thermal metamaterials.[32] The past decade has witnessed tremendous innovative methods and progress about thermal metamaterials designing in the interests of achieving heat flux manipulation, for example, combining copper or different alloy with polyurethane,[26] PDMS,[27] or polystyrene[28] to satisfy the thermal conductivity required. Furthermore, studies concerning thermal invisibility integrate with different functions like unconventional thermal cloak,[33] adaptive thermal cloaking,[34] omnidirectional camouflage device in thermal-electric field,[35] and so forth have been advanced as well. More profound researches about thermal metamaterials and metadevices can be found in the reviews.[36,37] Although enormous progress has been achieved in thermal cloaking by heat conduction, heat transfer problems dominated by heat convection[38,39] have, however, been rarely studied in depth so far.

To overcome this challenge, numerous research studies have been carried out in hydrodynamic metamaterials through transformation theory and Darcy's law in porous media.[40,41] On the basis of these studies, a surge in hydrodynamic metamaterials investigations[42–48] has emerged by virtue of transformation hydrodynamics,[42,43,47,48] scattering cancellation method,[44] convection-diffusion-balance method,[45] coupling electro-osmosis method,[46] and so forth. More comprehensive investigations of hydrodynamic

[1]School of Mechanical and Power Engineering, East China University of Science and Technology, Shanghai 200237, China

[2]Department of Physics, State Key Laboratory of Surface Physics, and Key Laboratory of Micro and Nano Photonic Structure (MOE), Fudan University, Shanghai 200438, China

[3]Lead contact

*Correspondence: bwang@ecust.edu.cn (B.W.), wangxs@ecust.edu.cn (X.W.), jphuang@fudan.edu.cn (J.H.)

https://doi.org/10.1016/j.isci.2022.105461

metamaterials can be found in the review.[49] These investigations have boosted the development of hydrodynamic metamaterials significantly, promoted the progress of drag reduction technology under creeping viscous potential flows with Reynolds numbers approximately one,[42] and paved the path for the extension of thermal cloaking from pure thermal conduction to convective heat transfer as well.

On the basis of the research studies in thermal and hydrodynamic metamaterials, transformation heat transfer has been proposed in porous media[50,51] and nonporous media,[52,53] respectively. Transformation heat transfer, as its name indicates, can lay the foundation for manipulating heat flux and fluid motion simultaneously. However, inhomogeneous or anisotropic parameters imposed from transformation theory have challenged the metamaterial fabrications on experimental levels.

Fortunately, by converting the energy transports equation to the Laplace equation to solve the analytical solution, convective cloaks composed of homogeneous and isotropic materials for creeping flows in porous[54] and for creeping viscous potential flows in nonporous media[55] have recently been proposed to hide the influence of both heat flux and velocity fields generated by the object, which immensely reduce the experimental fabrication of thermal metamaterials. However, the pressure is almost physically independent on the temperature under forced convective heat transfer, namely, it is the one-way coupling problem. This implies that forcing a nonlinear equation into a Laplace equation is generally applicable in extreme circumstances.[54–56] In addition, previous investigations generally focus on the performances of convective thermal cloaks in creeping viscous potential flows, but related studies in non-creeping viscous potential flows that weigh equally importantly in nature have not been intensively investigated.

To conquer these challenges, we have utilized the separation of variables method and proposed an equivalent-medium integral method to analytically deduce the parameters of convective thermal cloaks with homogenous and isotropic dynamic viscosity and thermal conductivity. The numerical simulations have demonstrated that these convective thermal cloaks can hide objects by manipulating heat fluxes and velocities for thermal non-creeping viscous potential flows. Besides, we have discovered these convective thermal cloaks appear the drag-free characteristics at various Reynolds numbers, and this characteristic still holds even the Reynolds number increases to 100.

RESULTS AND DISCUSSION

The function of convective thermal cloaks should not be affected when the properties, especially the thermal conductivity and heat source, of the hidden object alters. For this purpose, an adiabatic layer composed of impermeable and adiabatic materials should be applied on the surface of the hidden object first. Consequently, the design of the cloaking layer merely needs to counteract the convective heat transfer caused by the adiabatic wall, regardless of the variations of the object's parameters. As shown in Figure 1, the system consists of the cloaking layer ($R_1 < r \leq R_2$, region III), the adiabatic layer ($R_0 < r < R_1$, region II), and the object ($0 < r < R_0$, region I). The convective thermal cloaks, the adiabatic layer, and the object are submerged in a freestream ($r > R_2$, region IV) steadily. The geometric size of the whole system is height (H) × width (W) × depth (D), herein, D denotes total depth of the system along Z axis. Considering the object and the adiabatic layer are both impermeable to thermal fluid, we treat the hidden object and adiabatic layer as a whole.

To counteract the convective heat transfer caused by the adiabatic wall, we need to regulate the dynamic viscosity and thermal conductivity of the convective thermal cloaks. The specific expression of dynamic viscosity and thermal conductivity of cloaking layer ($R_1 < r \leq R_2$, region III) are $\mu_c = \frac{R_2^2 - R_1^2}{R_2^2 + R_1^2}\mu_b$ and $k_c = \frac{R_2^2 + R_1^2}{R_2^2 - R_1^2}k_b$, respectively. Herein, symbols μ_b and k_b represent the dynamic viscosity and thermal conductivity of working flow in background (region IV). The detailed solution of dynamic viscosity and deduction of thermal conductivity are presented in STAR Methods.

To validate the convective thermal cloaks performances, computational simulations are conducted on the basis of Equations 1, 2, and 3 in STAR Methods using commercial software COMSOL Multiphysics. Because the adiabatic layer, region II in Figure 1, is thermally insulated, impermeable and nonslip, the equivalent perturbations of this layer to the exterior fields mathematically equal to that of an adiabatic, impermeable, and nonslip wall located in $r = R_1$ in computational domain. For simplification, we numerically remove the adiabatic layer (region II) and the object (region I) (consider them as a whole), and replace them with an adiabatic, impermeable, and nonslip wall in $r = R_1$ in computational domain.

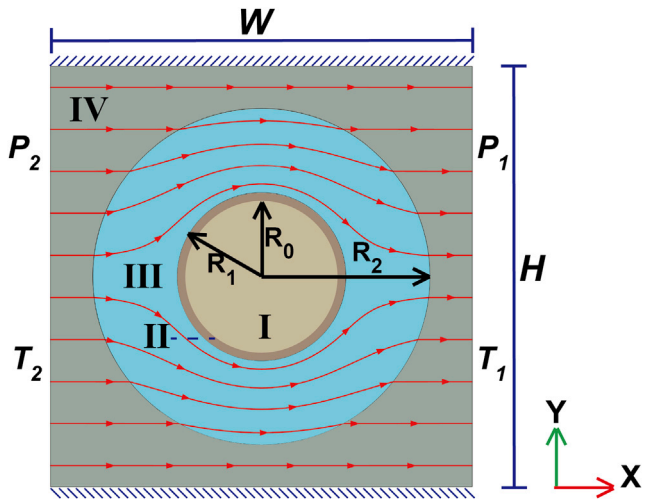

Figure 1. Schematic illustration of the convective thermal cloaks

Two-dimensional (2D) model with height (H) × width (W) = 2 cm × 2 cm, where R_0 = 3.5 mm, R_1 = 4 mm and R_2 = 8 mm represent the outer radius of the object, adiabatic layer, and cloaking layer of the convective thermal cloaks, respectively.

According to the geometric sizes of the computational domain where $H \times W \times D = 2\text{cm} \times 2\text{cm} \times 50\text{um}$, it is clear that $D \ll W$ and H, with which the incoming flow can be perceived two-dimensional flow known as Hele-Shaw flow.[57,58] The whole system, as shown in Figure 1, subjects to left-to-right Dirichlet boundary conditions with $\Delta T = 50K$ ($T_2 > T_1$). The incoming velocity of the freestream (region IV) is predetermined by pressure gradient of $\Delta p = 2Pa$ ($p_2 > p_1$) in the x direction, and the surfaces of all solid walls in the domain within $y = \pm 0.5H$, $z = \pm 0.5D$ and $r = R_1$ are dealt as adiabatic and nonslip boundary conditions. Related parameters used in numerical simulation, i.e., thermal properties of each region are presented in Table 1.

For clarity, the pure background flow is defined as background case, and object-existent case indicates the object and the adiabatic layer exist in the flow. Cloak case denotes convective thermal cloaks are applied on the object-existent case.

Prior to presenting the results of the cloak case, two comparison cases are introduced first. Figures 2A, 2D, 2B, and 2E demonstrate velocity and temperature fields of the background case and object-existent case, respectively. When the object is absent, the streamlines, isobars, and isotherms appear as straight lines (Figures 2A and 2D). As the object covered with an adiabatic layer is placed in the thermal fluid field, adiabatic surface at the solid wall impedes the flow of fluid and heat flux, which distort the isobars, streamlines, and isotherms outside the object (Figures 2B and 2E).

In Figures 2C and 2F, when the convective thermal cloaks are applied, the incoming fluid flow and heat flux are guided by the cloaks with higher velocity to counteract interference from objects covered with an adiabatic layer. In so doing, the disturbed velocity and temperature fields outward of the cloaks eventually restore, which appears exactly identical with velocity and temperature profiles of the background case.

In order to check the velocity and temperature differences between the cloak case and background case, we present the differences of velocity and temperature profiles by the cloak case subtracting those of the background case, (Figures 3A and 3B). Overall, the differences outside the cloaks tend to be zero.

Table 1. Thermal properties of each region in convective thermal cloaks

	c_p[J /(kg ·K)]	ρ[kg /m^3]	μ[Pa ·s]	k[W /(m ·K)]
Adiabatic layer in r = R_1 (regions I and II)			N/A	0
Background (water, region IV)	4179	997.1	10^{-3}	0.613
Cloaking layer (region III)	4179	997.1	6×10^{-4}	1.0217

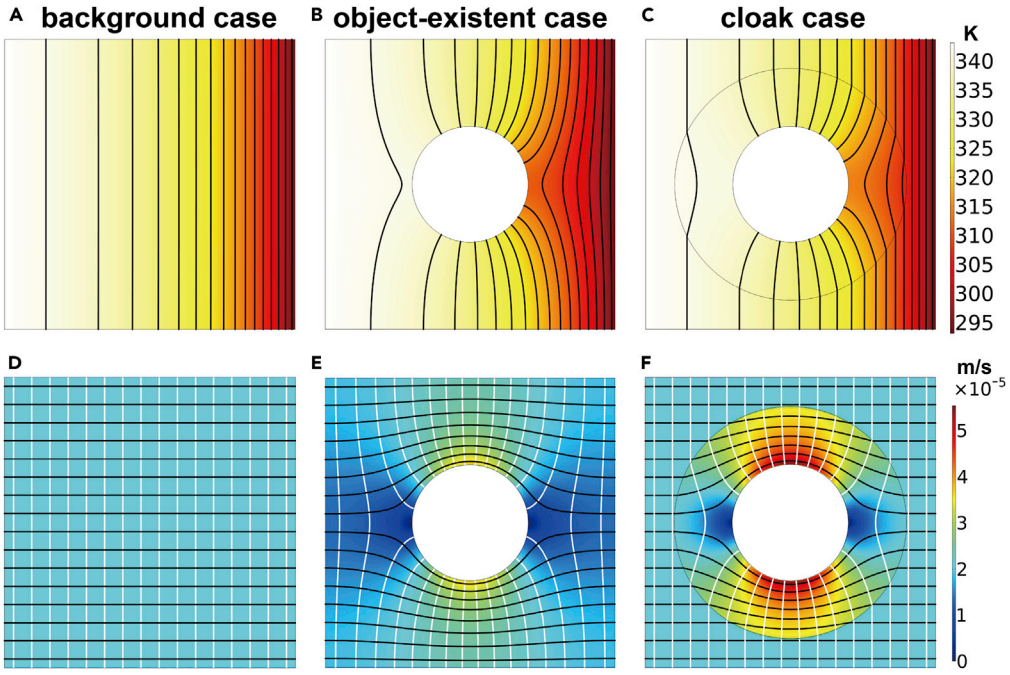

Figure 2. Velocity and temperature distributions

Velocity profiles superimposed with streamlines (black color) and isobars (white color). Temperature profiles superimposed with isotherms (black color).

(A–C) Temperature distributions of the background case, object-existent case, and cloak case.

(D–F) Velocity distributions of the background case, object-existent case, and cloak case.

To further quantitatively examine the validity of the convective thermal cloaks, the velocity distributions versus y/R_2 at $x = 0$, $x = -\frac{1}{4}W$, and $x = -\frac{9}{20}W$ are presented in Figure 3C, as well as temperature distributions versus x/R_2 at $y = 0$, $y = \frac{1}{4}H$, and $y = \frac{9}{20}H$ in Figure 3D. Both distributions outside cloaks ($|y/R_2| \geq 1$ or $|x/R_2| \geq 1$) appear invariant in conformity with those in the background case (black lines), proving the cloaks manage to eliminate the perturbations. Namely, the object submerged in the thermal fluid cannot be detected thermally and hydrodynamically.

Because forces work against each other, an object moves in a thermal flow field without disturbing the surrounding velocity fields and temperature fields, suggesting that the object probably is not subjected to drag forces when it becomes cloaking.

To quantitatively analyze the drag forces on the object and on the object wrapped with the cloak, we present their drag forces and drag reduction effects at various Reynolds numbers in Figure 4. Herein, Reynolds number can be defined as $Re = \frac{\rho U_{in} D}{\mu}$, where ρ, U_{in}, and μ represent the density, inlet velocity, and dynamic viscosity of the fluid, and D denotes the total depth of the system along the Z axis.

In this paper, Drag forces are calculated based on formula[43] of $F_d = \iint_S \left\{ \mu \left[\left(\frac{\partial u}{\partial y} + \frac{\partial v}{\partial x} \right) + 2\frac{\partial u}{\partial x} + \left(\frac{\partial u}{\partial z} + \frac{\partial w}{\partial x} \right) \right] + p_x \right\} dS$, where μ is the dynamic viscosity of water at room temperature, p_x is the pressure applied on X axis, and u , v, and w are velocity components in x, y, and z direction, respectively. S is the surface area of the adiabatic layer for the object-existent case, and that of cloaks for the cloak case.

Since the fluid flows across the walls of the channel itself generating a drag force, we consider the background case as a reference point. Figure 4A presents the variation of the relative drag force with Re for the object-existent case and cloak case. Figure 4B shows the drag reduction effect that is calculated by formula $\frac{(F_o - F_c)}{F_o} \times 100\%$, where F_o and F_c signify the drag force that the object and the object covering the cloak bear, respectively. It is noteworthy that the drag reduction effect is above 98%, representing

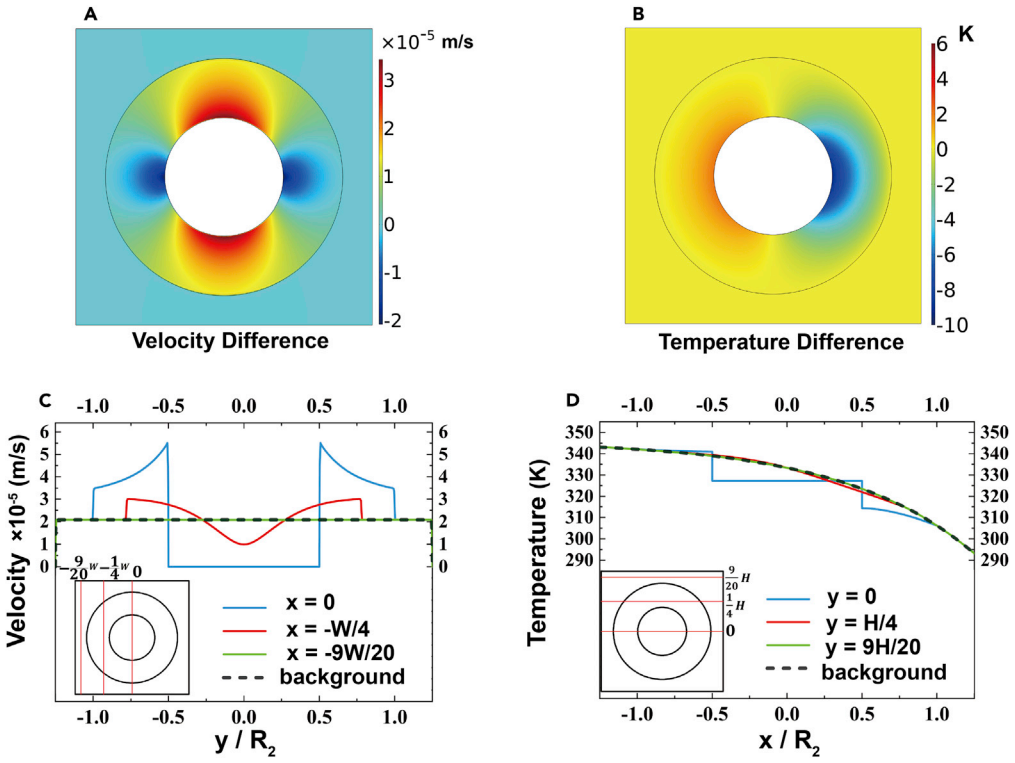

Figure 3. Comparisons of velocity and temperature distributions between the background case and cloak case

Velocity and temperature distributions of the background case with the black dashed lines are chosen as the references.

(A and B) Velocity and temperature differences between the cloak case and background case.

(C) Velocity distributions of the cloak case versus y / R_2 at $x = 0$, $x = -\frac{1}{4} W$, and $x = -\frac{9}{20} W$.

(D) Temperature distributions of the cloak case versus x / R_2 at $y = 0$, $y = \frac{1}{4} H$, and $y = \frac{9}{20} H$.

the vast majority of the drag force is eliminated, in spite of the increase of Reynolds numbers, even it increases to 100. Comparing with the previous study[42] that the nearly zero-drag effect holds where the Reynolds number is around one, our cloaks manage to increase the Reynolds number approximate 100 times. Namely, these convective thermal cloaks have tremendous potential in drag reduction effect under higher Reynolds numbers.

To further compare the performances of our cloaks with other convective thermal cloaks, we present the cloaking performance of three cloaks, i.e., ten-layer anisotropic-homogeneous (AH) convective thermal cloaks[52] (Figures 5C and 5F), anisotropic-inhomogeneous (AI) convective thermal cloaks[52] (Figures 5D and 5G), and isotropic-homogeneous (IH) cloaks (Figures 5E and 5H).

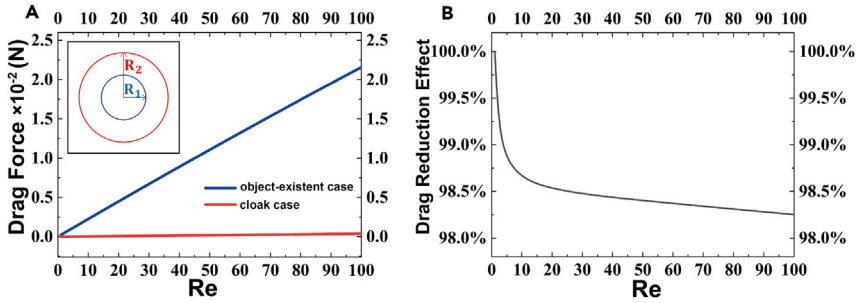

Figure 4. Drag force and drag reduction effect

(A) Drag force that the objects bear in the object-existent case and cloak case.

(B) Drag reduction effect of convective thermal cloaks at various Reynolds numbers.

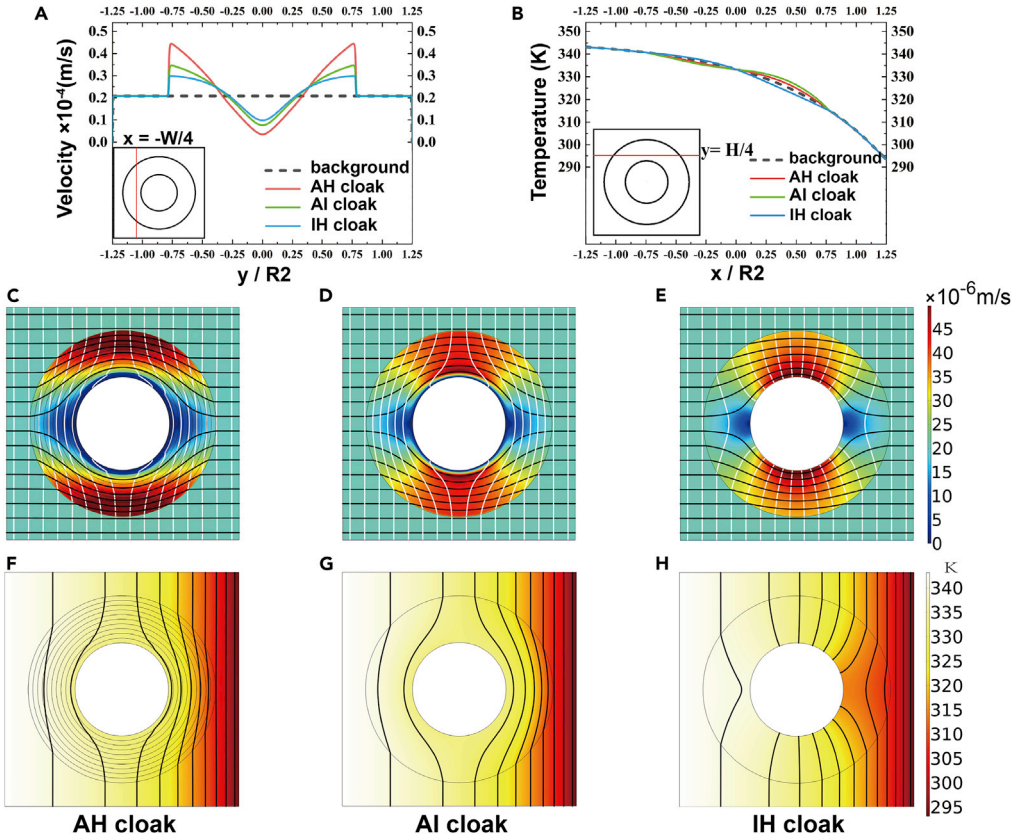

Figure 5. Velocity and temperature distributions for three different convective thermal cloaks

Velocity profiles superimposed with streamlines (black color) and isobars (white color). Temperature profiles superimposed with isotherms (black color).

(A) Velocity distributions versus y / R_2 at $x = -\frac{1}{4}W$ for three different cloaks.

(B) Temperature distributions versus x / R_2 at $y = \frac{1}{4}H$ for three different cloaks.

(C and F) Velocity and temperature distributions contours for ten-layer anisotropic-homogeneous (AH) convective thermal cloaks.

(D and G) Velocity and temperature distributions contours for anisotropic-inhomogeneous (AI) convective thermal cloaks.

(E and H) Velocity and temperature distributions contours for isotropic-homogeneous (IH) cloaks proposed in this letter.

As a fair comparison, AI cloaks and AH cloaks are modeled the same geometric size as IH cloaks. Considering that the former two cloaks are designed in creeping viscous potential flows, the incoming flowing are simplified as Stokes flow where IH cloaks still work well. Inlet velocity is predetermined by $\Delta p = 2\,Pa\,(p_2 > p_1)$, and other boundary conditions match the previous ones identically.

It seems that perturbations are eliminated by cloaks with demonstration in Figures 5C–5H. To further compare these three cloaks quantitatively, velocity distributions versus y/R_2 at $x = -\frac{1}{4}W$ and temperature distributions versus x/R_2 at $y = \frac{1}{4}H$ are presented in Figures 5A and 5B. In spite of the differences inside the cloaks, the distributions outside of the three cloaks appear invariant in conformity with those in the background (black lines), signifying all of them manage to eliminate the distortions for thermo-hydrodynamic fields. However, when it comes to experimental realization, IH cloaks prevail over AI cloaks and AH cloaks benefited from its isotropic-homogeneous parameters, dynamic viscosity, and thermal conductivity, required.

Conclusions

By utilizing the separation of variables method and equivalent-medium integral method, convective thermal cloaks with homogenous and isotropic dynamic viscosity and thermal conductivity are designed. Based on numerical simulation, we demonstrate convective thermal cloaks can manipulate thermal and

hydrodynamic fields simultaneously for non-creeping viscous potential flows and significantly prevent the interplay between the hidden object and exterior fields through quantitative analyses. In addition, we discover our cloaks appear the drag-free characteristics at various Reynolds numbers. Finally, by comparing with different convective thermal cloaks based on transformation heat transfer, we find out that the cloaks proposed in this study also have excellent manipulation on heat flux and fluid flow. Our investigation may considerably reduce the difficulties of cloak fabrications and lay foundation for the development of drag reduction technology under higher Reynolds numbers.

Limitation of the study

Although we have successfully demonstrated our cloaks through numerical simulations, our cloaks still possess limitations. First, the simultaneous manipulations of the thermal conductivity and the dynamic viscosity of the cloaks are filled with enormous challenges experimentally. Second, our cloaks are only effective at a moderate range of Reynolds numbers and are not applicable at higher Reynolds numbers or even turbulent circumstances, which are mainly influenced by the convective term in momentum transport equation. If in the future we can provide external fields on this basis to control the effects produced by the convective term, it may help us to promote the convective thermal cloaks to higher Reynolds number fields.

STAR★METHODS

Detailed methods are provided in the online version of this paper and include the following:

- KEY RESOURCES TABLE
- RESOURCE AVAILABILITY
  - Lead contact
  - Materials availability
  - Data and code availability
- EXPERIMENTAL MODEL AND SUBJECT DETAILS
- METHOD DETAILS
  - Isotropic and homogeneous dynamic viscosity of convective thermal cloaks
  - Isotropic and homogeneous thermal conductivity of convective thermal cloaks
- QUANTIFICATION AND STATISTICAL ANALYSIS

ACKNOWLEDGMENTS

This work is supported by Shanghai Science and Technology Development Funds (Grant No. 22YF1410600), by the National Natural Science Foundation of China (Grants No. 12205102, No. 11725521 and No. 12035004), and by the Science and Technology Commission of Shanghai Municipality (Grant No. 20JC1414700).

AUTHOR CONTRIBUTIONS

N.Y., H.W., B.W., and J.H. conceived the idea and designed the frame. N.Y. wrote the first draft of the manuscript. B.W., X.W., and J.H. commented the manuscript. N.Y., H.W., B.W., X.W., and J.H. edited and revised the manuscript.

DECLARATION OF INTERESTS

The authors declare no competing interests.

Received: September 11, 2022
Revised: October 13, 2022
Accepted: October 26, 2022
Published: November 18, 2022

REFERENCES

1. Li, T.-Q., Xu, Z.-H., Hu, Z.-J., and Yang, X.-G. (2010). Application of a high thermal conductivity C/C composite in a heat-redistribution thermal protection system. Carbon *48*, 924–925. https://doi.org/10.1016/j.carbon.2009.10.043.

2. Mao, Z., Wang, W., Liu, Y., Zhang, L., Xu, H., and Zhong, Y. (2014). Infrared stealth property based on semiconductor (M)-to-metallic (R) phase transition characteristics of W-doped VO2 thin films coated on cotton fabrics. Thin Solid Films *558*, 208–214.

3. Xu, R., Wang, W., and Yu, D. (2019). A novel multilayer sandwich fabric-based composite material for infrared stealth and super thermal insulation protection. Compos. Struct. *212*, 58–65. https://doi.org/10.1016/j.compstruct.2019.01.032.

4. Chen, L., Ren, Z., Liu, X., Wang, K., and Wang, Q. (2021). Infrared-visible compatible stealth based on Al-SiO2 nanoparticle composite film. Opt Commun. *482*, 126608. https://doi.org/10.1016/j.optcom.2020.126608.

5. Baranwal, N., and Mahulikar, S.P. (2014). Aircraft engine's infrared lock-on range due to back pressure penalty from choked convergent nozzle. Aero. Sci. Technol. *39*, 377–383. https://doi.org/10.1016/j.ast.2014.09.020.

6. Baranwal, N., and Mahulikar, S.P. (2016). Infrared signature of aircraft engine with choked converging nozzle. J. Thermophys. Heat Tran. *30*, 854–862. https://doi.org/10.2514/1.T4641.

7. Dev, O., Dayal, S., Dubey, A., and Abbas, S.M. (2020). Multi-layered textile structure for thermal signature suppression of ground based targets. Infrared Phys. Technol. *105*, 103175. https://doi.org/10.1016/j.infrared.2019.103175.

8. Xu, Z., Han, Y., Ren, D., and Li, J. (2022). An approach of multistage connected ventilation cooling structure for armored vehicle thermal management. J. Therm. Sci. Eng. Appl. *14*, 021008. https://doi.org/10.1115/1.4051370.

9. Vaitekunas, D.A., and Kim, Y. (2013). IR Signature Management for the Modern Navy (SPIE), pp. 261–270.

10. Laleh, R.E., and Ghasemloo, N. (2014). Calculate thermal infrared intensity of the hull's military ship. J. Geogr. Inf. Syst. *06*, 317–329.

11. Pendry, J.B., Schurig, D., and Smith, D.R. (2006). Controlling electromagnetic fields. Science *312*, 1780–1782.

12. Leonhardt, U. (2006). Optical conformal mapping. Science *312*, 1777–1780.

13. Fan, C.Z., Gao, Y., and Huang, J.P. (2008). Shaped graded materials with an apparent negative thermal conductivity. Appl. Phys. Lett. *92*, 251907. https://doi.org/10.1063/1.2951600.

14. Guenneau, S., Amra, C., and Veynante, D. (2012). Transformation thermodynamics: cloaking and concentrating heat flux. Opt. Express *20*, 8207–8218. https://doi.org/10.1364/oe.20.008207.

15. Huang, J.-P. (2019). Theoretical Thermotics: Transformation Thermotics and Extended Theories for Thermal Metamaterials (Springer Nature).

16. Han, T., Yuan, T., Li, B., and Qiu, C.-W. (2013). Homogeneous thermal cloak with constant conductivity and tunable heat localization. Sci. Rep. *3*, 1593. https://doi.org/10.1038/srep01593.

17. Nguyen, D.M., Xu, H., Zhang, Y., and Zhang, B. (2015). Active thermal cloak. Appl. Phys. Lett. *107*, 121901.

18. Li, Y., Zhu, K.-J., Peng, Y.-G., Li, W., Yang, T., Xu, H.-X., Chen, H., Zhu, X.-F., Fan, S., and Qiu, C.-W. (2019). Thermal meta-device in analogue of zero-index photonics. Nat. Mater. *18*, 48–54.

19. Xu, L.-J., and Huang, J.-P. (2020). Active thermal wave cloak. Chinese Phys. Lett. *37*, 120501. https://doi.org/10.1088/0256-307x/37/12/120501.

20. Chen, T., Weng, C.-N., and Tsai, Y.-L. (2015). Materials with constant anisotropic conductivity as a thermal cloak or concentrator. J. Appl. Phys. *117*, 054904. https://doi.org/10.1063/1.4907219.

21. Shen, X., Li, Y., Jiang, C., Ni, Y., and Huang, J. (2016). Thermal cloak-concentrator. Appl. Phys. Lett. *109*, 031907.

22. Xu, G., Dong, K., Li, Y., Li, H., Liu, K., Li, L., Wu, J., and Qiu, C.-W. (2020). Tunable analog thermal material. Nat. Commun. *11*, 6028. https://doi.org/10.1038/s41467-020-19909-0.

23. Zhou, L., Huang, S., Wang, M., Hu, R., and Luo, X. (2019). While rotating while cloaking. Phys. Lett. *383*, 759–763. https://doi.org/10.1016/j.physleta.2018.11.041.

24. Yang, F., Tian, B., Xu, L., and Huang, J. (2020). Experimental demonstration of thermal chameleonlike rotators with transformation-invariant metamaterials. Phys. Rev. Appl. *14*, 054024.

25. Li, J., Li, Y., Cao, P.-C., Yang, T., Zhu, X.-F., Wang, W., and Qiu, C.-W. (2020). A continuously tunable solid-like convective thermal metadevice on the reciprocal line. Adv. Mater. *32*, 2003823. https://doi.org/10.1002/adma.202003823.

26. Narayana, S., and Sato, Y. (2012). Heat flux manipulation with engineered thermal materials. Phys. Rev. Lett. *108*, 214303.

27. Schittny, R., Kadic, M., Guenneau, S., and Wegener, M. (2013). Experiments on transformation thermodynamics: molding the flow of heat. Phys. Rev. Lett. *110*, 195901. https://doi.org/10.1103/PhysRevLett.110.195901.

28. Han, T., Bai, X., Gao, D., Thong, J.T.L., Li, B., and Qiu, C.-W. (2014). Experimental demonstration of a bilayer thermal cloak. Phys. Rev. Lett. *112*, 054302. https://doi.org/10.1103/PhysRevLett.112.054302.

29. Xu, H., Shi, X., Gao, F., Sun, H., and Zhang, B. (2014). Ultrathin three-dimensional thermal cloak. Phys. Rev. Lett. *112*, 054301. https://doi.org/10.1103/PhysRevLett.112.054301.

30. Han, T., Yang, P., Li, Y., Lei, D., Li, B., Hippalgaonkar, K., and Qiu, C.-W. (2018). Full-parameter omnidirectional thermal metadevices of anisotropic geometry. Adv. Mater. *30*, 1804019. https://doi.org/10.1002/adma.201804019.

31. Qin, J., Luo, W., Yang, P., Wang, B., Deng, T., and Han, T. (2019). Experimental demonstration of irregular thermal carpet cloaks with natural bulk material. Int. J. Heat Mass Tran. *141*, 487–490. https://doi.org/10.1016/j.ijheatmasstransfer.2019.06.092.

32. Wang, J., Dai, G., and Huang, J. (2020). Thermal metamaterial: fundamental, application, and outlook. iScience *23*, 101637. https://doi.org/10.1016/j.isci.2020.101637.

33. Gao, Y., and Huang, J.P. (2013). Unconventional thermal cloak hiding an object outside the cloak. EPL *104*, 44001. https://doi.org/10.1209/0295-5075/104/44001.

34. Zhu, Z., Ren, X., Sha, W., Xiao, M., Hu, R., and Luo, X. (2021). Inverse design of rotating metadevice for adaptive thermal cloaking. Int. J. Heat Mass Tran. *176*, 121417. https://doi.org/10.1016/j.ijheatmasstransfer.2021.121417.

35. Feng, H., Zhang, X., Zhang, Y., Zhou, L., and Ni, Y. (2022). Design of an omnidirectional camouflage device with anisotropic confocal elliptic geometry in thermal-electric field. iScience *25*, 104183. https://doi.org/10.1016/j.isci.2022.104183.

36. Li, Y., Li, W., Han, T., Zheng, X., Li, J., Li, B., Fan, S., and Qiu, C.-W. (2021). Transforming heat transfer with thermal metamaterials and devices. Nat. Rev. Mater. *6*, 488–507. https://doi.org/10.1038/s41578-021-00283-2.

37. Yang, S., Wang, J., Dai, G., Yang, F., and Huang, J. (2021). Controlling macroscopic heat transfer with thermal metamaterials: theory, experiment and application. Phys. Rep. *908*, 1–65. https://doi.org/10.1016/j.physrep.2020.12.006.

38. Xu, L., and Huang, J. (2020). Negative thermal transport in conduction and advection. Chinese Phys. Lett. *37*, 080502. https://doi.org/10.1088/0256-307x/37/8/080502.

39. Xu, L.J., Yang, S., and Huang, J.P. (2021). Controlling thermal waves of conduction and convection. Europhys. Lett. *133*, 20006.

40. Urzhumov, Y.A., and Smith, D.R. (2011). Fluid flow control with transformation media. Phys. Rev. Lett. *107*, 074501. https://doi.org/10.1103/PhysRevLett.107.074501.

41. Urzhumov, Y.A., and Smith, D.R. (2012). Flow stabilization with active hydrodynamic cloaks. Phys. Rev. E Stat. Nonlin. Soft Matter Phys. *86*, 056313. https://doi.org/10.1103/PhysRevE.86.056313.

42. Park, J., Youn, J.R., and Song, Y.S. (2019). Hydrodynamic metamaterial cloak for drag-free flow. Phys. Rev. Lett. *123*, 074502.

43. Park, J., and Song, Y.S. (2020). Assembling hydrodynamic cloaks to conceal complex objects from drag. J. Fluid Struct. *98*, 103136. https://doi.org/10.1016/j.jfluidstructs.2020.103136.

44. Tay, F., Zhang, Y., Xu, H., Goh, H., Luo, Y., and Zhang, B. (2022). A metamaterial-free fluid-flow cloak. Natl. Sci. Rev. *9*, nwab205.

45. Wang, B., Shih, T.-M., Xu, L., Dai, G., and Huang, J. (2021). Intangible hydrodynamic cloaks for convective flows. Phys. Rev. Appl. *15*, 034014. https://doi.org/10.1103/PhysRevApplied.15.034014.

46. Boyko, E., Bacheva, V., Eigenbrod, M., Paratore, F., Gat, A.D., Hardt, S., and Bercovici, M. (2021). Microscale hydrodynamic cloaking and shielding via electro-osmosis. Phys. Rev. Lett. *126*, 184502. https://doi.org/10.1103/PhysRevLett.126.184502.

47. Wang, H., Yao, N.-Z., Wang, B., and Wang, X.-S. (2022). Homogenization design and drag reduction characteristics of hydrodynamic cloaks. Acta Phys. Sin. *71*, 134703. https://doi.org/10.7498/aps.70.20220346.

48. Yao, N.-Z., Wang, H., Wang, B., and Wang, X.-S. (2022). Venturi-effect rotating concentrators and nonreciprocity characteristics based on transformation hydrodynamics. Acta Phys. Sin. *71*, 104701. https://doi.org/10.7498/aps.71.20212361.

49. Wang, B., and Huang, J. (2022). Hydrodynamic metamaterials for flow manipulation: functions and prospects. Chinese Phys. B *31*, 098101. https://doi.org/10.1088/1674-1056/ac7f8c.

50. Dai, G., Shang, J., and Huang, J. (2018). Theory of transformation thermal convection for creeping flow in porous media: cloaking, concentrating, and camouflage. Phys. Rev. E *97*, 022129. https://doi.org/10.1103/PhysRevE.97.022129.

51. Dai, G., and Huang, J. (2018). A transient regime for transforming thermal convection: cloaking, concentrating, and rotating creeping flow and heat flux. J. Appl. Phys. *124*, 235103.

52. Wang, B., Shih, T.-M., and Huang, J. (2021). Transformation heat transfer and thermo-hydrodynamic cloaks for creeping flows: manipulating heat fluxes and fluid flows simultaneously. Appl. Therm. Eng. *190*, 116726. https://doi.org/10.1016/j.applthermaleng.2021.116726.

53. Wang, H., Yao, N.-Z., Wang, B., Shih, T.-M., and Wang, X. (2022). Homogeneous Venturi-effect concentrators for creeping flows: magnifying flow velocities and heat fluxes simultaneously. Appl. Therm. Eng. *206*, 118012. https://doi.org/10.1016/j.applthermaleng.2021.118012.

54. Yeung, W.-S., Mai, V.-P., and Yang, R.-J. (2020). Cloaking: controlling thermal and hydrodynamic fields simultaneously. Phys. Rev. Appl. *13*, 064030. https://doi.org/10.1103/PhysRevApplied.13.064030.

55. Dai, G., Zhou, Y., Wang, J., Yang, F., Qu, T., and Huang, J. (2022). Convective cloak in hele-shaw cells with bilayer structures: hiding objects from heat and fluid motion simultaneously. Phys. Rev. Appl. *17*, 044006. https://doi.org/10.1103/PhysRevApplied.17.044006.

56. Qu, T., Wang, J., and Huang, J.P. (2021). Manipulating thermoelectric fields with bilayer schemes beyond Laplacian metamaterials. EPL *135*, 54004. https://doi.org/10.1209/0295-5075/ac1648.

57. Hele-Shaw, H.S. (1898). Flow of water. Nature *58*, 520.

58. Kundu, P.K., Cohen, I.M., and Dowling, D.R. (2015). Fluid Mechanics (Academic Press).

59. Gömöry, F., Solovyov, M., Souc, J., Navau, C., Prat-Camps, J., and Sanchez, A. (2012). Experimental realization of a magnetic cloak. Science *335*, 1466–1468. https://doi.org/10.1126/science.1218316.

60. Schlichting, H., and Kestin, J. (1961). Boundary Layer Theory (Springer).

61. Erhard, P., Etling, D., Muller, U., Riedel, U., Sreenivasan, K., and Warnatz, J. (2010). Prandtl-essentials of Fluid Mechanics (Springer Science & Business Media).

STAR★METHODS

KEY RESOURCES TABLE

REAGENT or RESOURCE	SOURCE	IDENTIFIER
Software and algorithms		
COMSOL Multiphysics	COMSOL Multiphysics 5.6	cn.comsol.com
Adobe illustrator	Adobe illustrator 2021	www.adobe.com

RESOURCE AVAILABILITY

Lead contact

Further information and requests for resources should be directed to and will be fulfilled by the lead contact, Bin Wang (bwang@ecust.edu.cn).

Materials availability

This study did not generate new unique reagents.

Data and code availability

- All data reported in this paper will be shared by the lead contact upon request.
- This paper does not report original code.
- Any additional information required to reanalyze the data reported in this paper is available from lead contact upon request.

EXPERIMENTAL MODEL AND SUBJECT DETAILS

Our study does not use experimental models typical in the life sciences.

METHOD DETAILS

Isotropic and homogeneous dynamic viscosity of convective thermal cloaks

For steady-state incompressible flow without the influence of body forces, continuum equations governing continuity, momentum transport, and energy transports can be written as

$$\nabla \cdot \boldsymbol{u} = 0 \quad \text{(Equation 1)}$$

$$\rho \boldsymbol{u} \cdot \nabla \boldsymbol{u} + \nabla p = \mu \nabla^2 \boldsymbol{u} \quad \text{(Equation 2)}$$

$$\rho c_p \boldsymbol{u} \cdot \nabla T = k \nabla^2 T \quad \text{(Equation 3)}$$

where $\boldsymbol{u}$, p and T are velocity, pressure and temperature respectively. Symbols ρ, μ, c_p and k signify the density, dynamic viscosity, heat capacity and thermal conductivity, respectively.

In light of the continuity equation and momentum equation are almost independent on temperature under forced convective heat transfer, which can be treated as the one-way coupling problem. Furthermore, heat flows can be manipulated via regulating dynamic viscosity and thermal conductivity in cloaking layer. Based on above two arguments, we first solve the continuity and momentum equations to obtain the dynamic viscosity. Then, thermal conductivity is deduced by virtue of the connections among velocity, dynamic viscosity and thermal conductivity in momentum and energy transports equations.

In the previous hydrodynamic cloaks,[45] under irrotational-flow idealization, Equations 1 and 2 can be transformed into the Laplace equations as

$$\nabla \cdot \nabla \varphi = 0 \quad \text{(Equation 4)}$$

$$\nabla \cdot \nabla \left(\mu^{-1} \nabla E \right) = 0 \quad \text{(Equation 5)}$$

where φ denotes the velocity potential meets $\boldsymbol{u} = \nabla\varphi$, and $E = \frac{1}{2}\rho|\boldsymbol{u}|^2 + p$. The term $\frac{1}{2}\rho|\boldsymbol{u}|^2$ in $E = \frac{1}{2}\rho|\boldsymbol{u}|^2 + p$derives from the nonlinear convective term $\boldsymbol{u}\cdot\nabla\boldsymbol{u}$ whose unit can be expressed as mechanical energy density (J/m^3). Further, Equations 4 and 5 can be unified into Equation 6, which bears the Laplace-equation form. Therefore, an analytical solution can be obtained[45] by separating variables.[28,59]

$$\nabla\cdot(\xi\nabla\Theta) = 0 \qquad \text{(Equation 6)}$$

where $\xi = (1, \mu^{-1})$, $\Theta = (\varphi, E)$.

The analytic solution of the Equation 6, $\nabla\cdot(\xi\nabla\Theta) = 0$, under cylindrical coordinate can be generally written as Equation 7.

$$\Theta_i = A_0^i + B_0^i \ln r + \sum_{m=0}^{\infty}\left[A_m^i \sin(m\theta) + B_m^i \cos(m\theta)\right] r^m + \sum_{m=0}^{\infty}\left[C_m^i \sin(m\theta) + D_m^i \cos(m\theta)\right] r^{-m} \qquad \text{(Equation 7)}$$

where A_0^i, B_0^i, A_m^i, B_m^i, C_m^i, and $D_m^i (i = I, II, III, IV)$ represent the coefficients determined by the specific boundary conditions.

According to the physical fields investigated in our research, and considering the corresponding boundary conditions constraints and finiteness of the computational domain, Equation 7 can be simplified as Equation 8.

$$\Theta_i = A_0^i + B_1^i r\cos\theta + C_1^i r^{-1}\cos\theta \qquad \text{(Equation 8)}$$

The Θ_i in Equations 7 and 8 signifies the solution in each region, $i = I$ and II denote the object coated with adiabatic layer ($0 < r \leq R_1$), $i = III$ denotes cloaking layer ($R_1 < r \leq R_2$), and $i = IV$ represents free-stream region ($r > R2$), respectively. Mathematically, the continuity condition in each interface can be expressed as

$$\begin{cases} \Theta_{I,II}\big|_{r=R_1} = \Theta_{III}\big|_{r=R_1} \\ \Theta_{III}\big|_{r=R_2} = \Theta_{IV}\big|_{r=R_2} \\ \xi_{I,II}\dfrac{\partial\Theta_{I,II}}{\partial r}\Big|_{r=R_1} = \xi_{III}\dfrac{\partial\Theta_{III}}{\partial r}\Big|_{r=R_1} \\ \xi_{III}\dfrac{\partial\Theta_{III}}{\partial r}\Big|_{r=R_2} = \xi_{IV}\dfrac{\partial\Theta_{IV}}{\partial r}\Big|_{r=R_2} \end{cases} \qquad \text{(Equation 9)}$$

By substituting Equations 8 into 9, the connection among the dynamic viscosity of different regions can be obtained as

$$\mu_h = \frac{\mu_c\cdot\left[R_2{}^2(\mu_b - \mu_c) + (\mu_b + \mu_c)R_1{}^2\right]}{(\mu_b + \mu_c)R_1{}^2 - R_2{}^2(\mu_b - \mu_c)}, \qquad \text{(Equation 10)}$$

where μ_b and μ_c signify the viscosity of fluid in background and cloaking layer of convective thermal cloaks, μ_h represents the effective viscosity of the object coated with the adiabatic layer (hidden object), R_1 and R_2 represent the outer radius of the adiabatic layer and cloaking layer, respectively.

Obviously, one of these three parameters is interdependent on the rest, namely, μ_c can be determined when μ_b and μ_h are given. In our research, setting water as the working fluid with viscosity μ_b = 1 mPa· s and density ρ = 997 kg/m^3 under room temperature. Because solid wall is generally treated as nonslip wall, μ_h can be treated as the infinity. Accordingly, on the basis of Equation 10, the viscosity of the convective thermal cloaks can be presented as

$$\mu_c = \frac{R_2^2 - R_1^2}{R_2^2 + R_1^2}\,\mu_b \quad R_1 < r \leq R_2 \qquad \text{(Equation 11)}$$

According to Equation 11, the value of μ_c merely relates to R_1, R_2 and μ_b, not to the spatial coordinates, which is identical to the expression for the dynamic viscosity of the cloak in reference.[45]

This consistency reflects the validity of Equation 10 when considering the nonslip wall of the object. Through the above derivation, the homogenous and isotropic dynamic viscosity has been obtained, and only the thermal conductivity of the cloaks is left to be deduced.

Isotropic and homogeneous thermal conductivity of convective thermal cloaks

To deduce the thermal conductivity of convective thermal cloaks, we utilize the connections among velocity, dynamic viscosity and thermal conductivity in momentum and energy transports equations. For clarity, the pure background flow is defined as background case, and object-existent case indicates the object and the adiabatic layer exist in the flow. Cloak case denotes convective thermal cloaks are applied on the object-existent case.

As stated above, forced convective heat transfer can be treated as the one-way coupling problem, due to the nearly complete independence of continuity equation and momentum equation on temperature. Moreover, because the relationship of the dynamic viscosity between the background case and the cloak case (Equation 11) has been settled, we will be able to further find the relationship between the velocity and the dynamic viscosity.

According to the geometric sizes where $D \ll W$ and H, the incoming flow can be perceived two-dimensional one known as Hele-Shaw flow.[57,58] Therefore, the global average velocity distributions of the background case can be expressed as[60,61]

$$u_1 = -\frac{D^2}{12\mu_1}\frac{dp_1}{dx} \quad \text{(Equation 12)}$$

where μ_1, u_1 and p_1 denote dynamic viscosity, velocity and pressure. Symbol D represents total depth of the system along Z-axis.

For the cloak case, with respect to velocity $\boldsymbol{u}_2$ inside the convective thermal cloaks, it varies with space, and whether it follows the Hele-Shaw flow pattern remains uncertain. Thus, we analyze the flow states in the peripheral area of convective thermal cloaks, namely, region IV at first. Comparing the flow patterns between the background case and cloak case, it should be claimed that the flow states in region IV of both cases must be identical, because velocity differences in region IV of the cloak case have been eliminated by regulating the dynamic viscosity of cloaking layer. Therefore, the effective flow states of regions I, II, III in the cloak case should follow the Hele-Shaw flow pattern to satisfy the region IV to preserve the Hele-Shaw flow pattern. Ulteriorly, on account of the velocity of regions I, II in cloak case equal zero and cylindrical objects are symmetric on the X-axis, the effective average velocity distributions of the cloak case in regions I, II, III can be represented by that in region III, and is expressed as[60,61]

$$u_{2,\,eff} = -\frac{D^2}{12\mu_2}\frac{dp_{2,\,eff}}{dx} \quad \text{(Equation 13)}$$

where μ_2, $u_{2,\,eff}$ and $p_{2,\,eff}$ denote dynamic viscosity, effective velocity and pressure. Symbol D represent the total depth of the system along Z-axis.

Here, what should be pointed out is that the term $\frac{dp_1}{dx}$ in regions I, II, III in Equation 12 and term $\frac{dp_{2,\,eff}}{dx}$ in Equation 13 are identical, since the overall flow states of regions I, II, III between the background case and cloak case conform with each other. From Equations 12 and 13, the connections between velocity and dynamic viscosity can be concluded as

$$\frac{u_1}{u_{2,eff}} = \frac{\mu_2}{\mu_1} \quad \text{(Equation 14)}$$

The above demonstrates the connections between velocity and dynamic viscosity through analyzing momentum equation, but thermal conductivity in energy transports equation has not been involved yet. Thus, we will analyze the energy transports equation. In fact, for the one-way coupled forced convective heat transfer, the convective heat transfer of the fluid is influenced by regulating the velocity affecting the momentum transport of the fluid. Therefore, there must be a connection between velocity and thermal conductivity. To find this connection, we first analyze the energy transports equation, which is shown in Equation 15, of the cloak case to obtain the thermal conductivity of convective thermal cloaks. Considering energy transported in regions I, II, III must obey the energy conservation law, we adopt the integral form of

energy transports equation in these regions. Besides, regions I, II in the cloak case are impermeable and adiabatic, then energy transported in these three regions can be represented by that of region III. Hence, this treatment is tentatively named "equivalent-medium integral method".

$$\rho c_p \iint \left(u_{2,eff} \frac{\partial T_{2,eff}}{\partial x} + v_{2,eff} \frac{\partial T_{2,eff}}{\partial y} \right) d\Omega_{III} = \iint k_{2,eff} \left(\frac{\partial^2 T_{2,eff}}{\partial x^2} + \frac{\partial^2 T_{2,eff}}{\partial y^2} \right) d\Omega_{III} \quad \text{(Equation 15)}$$

where $u_{2,eff}$, $v_{2,eff}$ and $T_{2,eff}$ represent the effective velocity components and temperature in region III. Symbols ρ, c_p and $k_{2,eff}$ signify the density, heat capacity and effective thermal conductivity respectively. In light of the fact that the whole thermal and flow fields are symmetric along the X-axis and the object is covered by impermeable adiabatic layer, terms $\iint v_{2,eff} \frac{\partial T_{2,eff}}{\partial y} d\Omega_{III}$ and $\iint \frac{\partial^2 T_{2,eff}}{\partial y^2} d\Omega_{III}$ in Equation 15 equal zero, and effective thermal conductivity $k_{2,eff}$ and effective velocity u_{2eff} are constant, Equation 15 can be further simplified as

$$\rho c_p u_{2,eff} \iint \frac{\partial T_{2,eff}}{\partial x} d\Omega_{III} = k_2 \iint \left(\frac{\partial^2 T_{2,eff}}{\partial x^2} \right) d\Omega_{III} \quad \text{(Equation 16)}$$

Here, $T_{2,eff}$ denotes the general temperature distributions of the region III in cloak case, which is similar to the role of $u_{2,\ eff}$ in momentum equation. To ensure the temperature distributions outside region III is undisturbed, the temperature distributions of the cloak case and the background case should be compared. Similarly, the whole thermal and flow fields are symmetric on the X-axis, thus components along Y-axis such as $\iint v_1 \frac{\partial T_1}{\partial y} d\Omega_{I,II,III}$ and $\iint \frac{\partial^2 T_1}{\partial y^2} d\Omega_{I,II,III}$ are cancelled. Consequently, the analyses of energy transports equation in the background case are performed next.

$$\rho c_p u_1 \iint \frac{\partial T_1}{\partial x} d\Omega_{I,II,III} = k_1 \iint \frac{\partial^2 T_1}{\partial x^2} d\Omega_{I,II,III} \quad \text{(Equation 17)}$$

Equation 17 expresses the energy transports of the background case in regions I, II, III. Where u_1 and T_1 represent the velocity and temperature respectively. Symbols ρ, c_p and k_1 signify the density, heat capacity and thermal conductivity, respectively.

What should be noted is, once again, that the precondition for the consistent temperature distributions outside region III in both cases is the global temperature distributions in regions I, II, III should be identical in both cases. Namely, term $\iint \frac{\partial T_{2,eff}}{\partial x} d\Omega_{III}$ in Equation 16, and term $\iint \frac{\partial T_1}{\partial x} d\Omega_{I,II,III}$ in Equation 17 equals to each other. Likewise, $\iint \frac{\partial^2 T_{2,eff}}{\partial x^2} d\Omega_{III}$ in Equation 16 and $\iint \frac{\partial^2 T_1}{\partial x^2} d\Omega_{I,II,III}$ in Equation 17 are equivalent.

Accordingly, by comparing Equations 16 and 17, we obtain

$$\frac{u_1}{u_{2,eff}} = \frac{k_1}{k_2} \quad \text{(Equation 18)}$$

According to Equation 18, we know that the cloaking function is achieved by the interrelationship of the velocity and the thermal conductivity.

Up to now, the correlations between velocity and dynamic viscosity Equation 14, and that between velocity and thermal conductivity Equation 18 are obtained. Eventually, bridged by velocity in the background case and cloak case, the relationship between thermal conductivity and dynamic viscosity can be obtained as below.

$$\frac{k_1}{k_2} = \frac{\mu_2}{\mu_1} \quad \text{(Equation 19)}$$

Therefore, specific expression for thermal conductivity of convective thermal cloaks can be achieved combing Equations 11 and 19, and is expressed as Equation 20. For the sake of understandability, the subscript of k_2 is replaced with the initials of "cloak" (k_c), the subscript of k_1 is replaced with the initials of "background" (k_b).

$$k_c = \frac{R_2^2 + R_1^2}{R_2^2 - R_1^2} k_b \ R_1 < r \leq R_2 \quad \text{(Equation 20)}$$

Instead of spatial coordinates, it is thermal conductivity of working flow k_b and geometric parameters R_1 and R_2 that determine the cloaks' thermal conductivity k_c. Namely, thermal conductivity of cloaks is isotropic and homogenous as well.

It is noteworthy that the results of Equation 20 are coincident with those in study[28] for the thermal conductive cloak. This can be comprehended from following perspectives. Under forced convective heat transfer, thermal energy is transported by thermal conduction and thermal convection simultaneously. In Hele-Shaw flows, the convection has already been manipulated by regulating dynamic viscosity. Hence, the energy transported by thermal convection, influenced by fluid motion, is regulated correspondingly (namely the part of the convection cloaking is achieved), and only thermal conduction part in convective heat transfer left to be solved. Therefore, the thermal conductivity of our cloak is in accord with study[28] when applying an impermeable adiabatic layer around the hidden object.

To summarize, Equations 11 and 20 represent the parameters of the convective thermal cloak that couple thermal convection and thermal conduction, by which we can realize the cloaking of the object in the temperature and velocity fields. Through these two parameters, we can know that the convective thermal cloak regresses to a hydrodynamic cloak[45] when heat transfer is not considered, and the thermal convective cloak regresses to a thermal conductive cloak[28] when convection is not considered.

QUANTIFICATION AND STATISTICAL ANALYSIS

Our study does not include quantification or statistical analysis.